RSC Advances



This is an *Accepted Manuscript*, which has been through the Royal Society of Chemistry peer review process and has been accepted for publication.

Accepted Manuscripts are published online shortly after acceptance, before technical editing, formatting and proof reading. Using this free service, authors can make their results available to the community, in citable form, before we publish the edited article. This Accepted Manuscript will be replaced by the edited, formatted and paginated article as soon as this is available.

You can find more information about *Accepted Manuscripts* in the **Information for Authors**.

Please note that technical editing may introduce minor changes to the text and/or graphics, which may alter content. The journal's standard <u>Terms & Conditions</u> and the <u>Ethical guidelines</u> still apply. In no event shall the Royal Society of Chemistry be held responsible for any errors or omissions in this *Accepted Manuscript* or any consequences arising from the use of any information it contains.



Hydroxyapatite conjugated Graphene Oxide nanocomposite: A new sight for significant application in adsorption

Triveni Kumar Mahto, Subhas Chandra Pandey, Soumen Chandra, Amit Kumar, Sumanta kumar Sahu*

Department of Applied Chemistry, Indian School of Mines, Dhanbad 826004, Jharkhand, India

* To whom correspondence should be addressed. E-mail:<u>sumantchem@gmail.com</u>,

<u>sahu.s.ac@ismdhanbad.ac.in;</u> Fax: +91-326-2307772; Tel: +91-326-2235936

ABSTRACT

Great efforts have been made to develop efficient adsorbent in recent years. In this work, graphene oxide (GO) was synthesized and the surface chemistry of GO was modified by means of hydroxyapatite (HAP) conjugation in order to increase the number of active sites responsible for cationic dye adsorption. The obtained HAP conjugated GO nanocomposites were characterized using various techniques such as FTIR, RAMAN, XRD, TGA, FESEM, BET surface area and AFM. Here malachite green (MG) was used as a model dye and the effect of several parameters like time, pH, temperature, adsorbent dose, and MG concentration on adsorption were investigated. The isotherm, kinetic and thermodynamic parameters were measured. The adsorption of MG was best described by freundlich isotherm with pseudo second order kinetic model. In addition, the removal efficiency was maintained at 82 % even in fourth cycle, which supported the reusability and stability of fabricated nanocomposite for cationic dye adsorption from aqueous medium.

1. INTRODUCTION

Adsorption process has been recognized as one of the most straightforward, effective and efficient strategy in removing a variety of pollutants from contaminated water. 1-2 With rapid advancements in nanotechnology and nanoscience, graphene oxide and its composites, as an adsorbent, are extensively studied for the removal of a variety of pollutants.³⁻⁴ Although other adsorbents such as mesoporous silica⁵, activated carbon⁶, polymers¹, magnetic nanocomposites² etc are widely investigated since decades with varying level of success. GO sets a new dimension in the field of environmentology. GO is a single layered sheet of carbon atoms with honeycomb like structure and this unique structure endows rich in O- functionalities⁷ such as hydroxyl and epoxy groups on its basal plane and carboxyl and carbonyl groups at the edges of the nanosheets.8 The O- functionalities act as anchoring sites for nucleation and growth of different nanoparticles.9 However the blocking of O- functionalities of GO after nucleation and growth of nanoparticles might lead to reduce its application in adsorption technology. So the selection of nanoparticles for nucleation and growth onto the surface of GO is an important issue while the strategy of synthesis of GO based nanocomposites are made for adsorption as well as photocatalysis. Here we have chosen HAP because it has great value and significance due to its biocompatibility¹⁰, binding affinity¹¹, and low cost¹², and has been investigated for application in tissue engineering, bone repair, and protein¹³, drug and gene delivery. ¹⁴ Despite of its wide variety of potential applications in biological ground, hydroxyapatite has emerged as one of the most reliable adsorbent biomaterial because it has displayed good cytocompatibility as have been experimentally proven in many research. 15-16 Different pollutants including cyanide 17, phenol 18, congo red¹⁹ and heavy metal ions²⁰ have been removed from environment using HAP based

composites. HAP is also suitable candidate for establishing bond with organic molecules of different size. Recently few research works have been devoted to the fabrication of GO and HAP composites for potential application. For instance Li et al reported that Ti substrate coated with GO/HA composites not only showed superior in vitro biocompatibility but also higher corrosion resistance in comparison with HA coated and uncoated Ti substrate were observed²¹. Gao et al coated AZ91 magnesium alloy with HA/GO hybrid and improved corrosion resistance of Mg alloys was achieved.²² However, till date there is no report of dye adsorption using GO/HAP nanocomposites. So the target of the present study is to fabricate HAP conjugated GO (GO/HAP) nanocomposites for dye adsorption. Here malachite green (MG) is chosen as a model dye, because it is tinctorially strong synthetic dye with the most controversy.²³ Their arrival to environment causes fertility reduction in living being, carcinogenic and mutagenic.

2. EXPERIMENTAL

2.1.Materials.

Graphite powder (APS 7-11 micron, 99%), and Calcium nitrate tetrahydrate (99%) were purchased from Alfa Aesar (A Johnsan Matthey Company). KMnO₄, H₂SO₄, FeCl₃ (anhydrous), FeSO₄·7H₂O, Ammonia solution, Ammonium dihydrogen phosphate and Malachite Green were acquired from Merck India. These chemicals were used as received. Millipore distilled water was used throughout the experiments.

2.2. Synthesis of GO

The oxidation of graphite powder to synthesize GO was performed according to improved Hummer's method with a little modification of reported method.²⁴⁻²⁵ Briefly, 1 g of graphite powder was dispersed into 23 ml concentrated H₂SO₄ and stirred half an hour to make

homogeneous. Then 3 g KMnO₄ was gradually added into the homogeneous mixture under continuous stirring and then the system was transferred to oil bath maintained at 50 °C. After 2 h stirring, 70 ml water was slowly added; consequently the solution temperature was raised, which was maintained at 98 °C for 15 minutes. The reaction was terminated by adding another 70 ml water and 5 ml H₂O₂ (30%). The solid product was collected and initially washed with 5% HCl and finally the product was repeatedly washed with water till the supernatant pH reached to neutral and dried for further modification.

2.3. Synthesis of HAP

HAP nanograins were synthesized under inert medium by wet precipitation method with some modification of previous reports. Calcium nitrate tetrahydrate and ammonium dihydrogen phosphate were used as the sole sources of calcium ions and phosphate respectively. In brief, stock solution (50 ml) of each calcium nitrate tetrahydrate (0.01 M) and ammonium dihydrogen phosphate (0.006 M) were prepared and stirred on 300 RPM for two hours. Thereafter, in argon atmosphere phosphate solution was added to nitrate solution with continuous stirring and temperature at 35 °C. In this stage the solution turned milky white. When the solution temperature reached to 60 °C aqueous ammonia was added and maintained the pH at 11. After 2 h vigorous stirring at 90 °C the thick milky white precipitate was cooled to room temperature and aged overnight. Finally the precipitate was collected, washed and dried for further application.

2.4. Synthesis of GO/HAP nanocomposites

A stock solution (50 ml) of calcium nitrate tetrahydrate was added drop wise into GO suspension over 30 minute with vigorous stirring. After 1 h, stock solution (50 ml) of ammonium dihydrogen phosphate was added dropwise under argon atmosphere and stirred for another 1 h at

35 °C. When the temperature reached to 60 °C, aqueous ammonia was added and pH was maintain at 11. The resultant dark brown dispersion was heated to 90 °C for 2 h, then the dark brown thick precipitate was cooled at room temperature and aged overnight. Finally the precipitate was filtered, washed and dried at 90 °C for further applications. In this work a series of nanocomposites were prepared by varying HAP precursors and these were labeled as GO/HAP-1, GO/HAP-2, and GO/HAP-3 respectively. Different amount of precursors for GO/HAP nanocomposites are listed in table 1.

Table 1: Experimental parameters for GO/HAP nanocomposites synthesis.

Sample	Molarity of S1 (M)	Amount of S1 (g)	Molarity of S2 (M)	Amount of S2 (g)	Amount of GO (g)	pН
GO/HAP-1	0.01	0.2361	0.006	0.0792	0.01	11
GO/HAP-2	0.02	0.4723	0.012	0.1584	0.01	11
GO/HAP-3	0.03	0.7084	0.018	0.2369	0.01	11

Note: [S1: Calcium nitrate tetrahydrate, S2: Ammonium dihydrogen phosphate]

2.5. Characterization techniques

The FTIR spectra were measured using Thermo Nicolet Nexux (model 870) FTIR spectrophotometer. The powder X-ray diffraction pattern was recorded on Philips PW 1710 X-ray diffractometer in scanning angle (2θ) ranged from 10 to 80°. The morphology was obtained from scanning electron microscopy (SEM) using a JEOL JEM1010 electron microscope. A Raman spectrum was recorded with a Nicolet Almega XR dispersive raman spectrometer using Nd:YAG laser source of wavelength 532 nm. Thermal decomposition analysis was carried out

with Perkin Elemer 1 DTA-TGA instrument under nitrogen flow. The surface area was investigated by BET method using Quantachrome NOVA 3200e instrument. Atomic force microscope image were obtained using Perkin Bruker Icon with scan analyst. The change in absorbance of MG was measured by UV-1800 spectrophotometer with operating voltage of 220-240V/50-60Hz (Shimadzu corporation).

2.6. MG adsorption analysis

Batch experiments were performed with GO/HAP-2 nanocomposites for the removal of MG from supplied aqueous solution. When necessary, the desired concentration of MG was prepared by diluting a stock solution of dye (100 mg L⁻¹) and used as soon as possible. For adsorption typically 0.01 g GO/HAP-2 as an adsorbent was immersed in 20 ml of desired MG solution and shaken at 110 rpm with Rivotek incubator shaker. The effect of influencing factors like time (0–90 minute), pH (2–10), temperature (303–323 K), dye concentration, and adsorbent dose were also investigated. After adsorption, the clear supernatant solution was collected and the concentration of MG remaining in the solution was determined through UV spectrophotometer at a wavelength of 617 nm. The extents of MG adsorptions on GO/HAP-2, in terms of percentage dye removal efficiency (R_e) and adsorption efficiency (q_e) were calculated by the following equation.¹

$$(R_e)\% = \frac{C_0 - C_e}{C_0} \times 100$$
 (1)

$$q_e = \frac{c_0 - c_e}{W} \times V \tag{2}$$

where C_0 and C_e are the initial and equilibrium liquid concentration in mg L^{-1} respectively. V is the volume of MG solution taken and W is the weight of GO/HAP-2 taken (g).

2.7. Dye desorption and reuse study

For desorption, the dye adsorbed GO/HAP-2 nanocomposites were dispersed in methanol solution containing 4 % acetic acid. After desorption the clear supernatant solution was collected and percentage dye desorption (D_e %) was calculated by the following equation

$$(D_e)\% = \frac{Dye \ desorbed \ (mg \ L^{-1})}{Dye \ adsorbed \ (mg \ L^{-1})} \times 100$$
 (3)

Similarly after desorption the GO/HAP-2 nanocomposites were collected, rinsed with water and then reused in the next cycle of adsorption. The percentage dye removal efficiency (Re %), in this case was calculated by equation 1.

3. RESULTS AND DISCUSSION

The various oxygen containing functionalities of GO acting as anchor sites and thus GO strongly absorb Ca²⁺ ions through electrostatic interaction and consequently the rate of nucleation of HAP on the surface of GO increases.²⁸ Here we have synthesized three types of GO/HAP nanocomposites with varying HAP precursors. The synthetic progress of GO/HAP nanocomposites starting from GO can be monitored by UV-VIS spectroscopy as shown in fig. 1a. The UV-VIS absorption peak of GO at 232 nm shifted to 263 nm with poor absorbance and the colour of the GO solution changed from light yellow to gray (fig. 1b), demonstrating that conjugation of HAP onto GO sheets took place and GO was slightly reduced. Among GO, HAP and varying GO/HAP nanocomposites, GO/HAP-2 showed the highest adsorption efficiency towards the adsorption of MG (Fig. S1, supporting information). So, the detail study was focused

on GO/HAP-2 only. The prime driving force of the adsorption of Dye onto GO/HAP-2 nanocomposites was the electrostatic interaction between the considerable quantities of negative sites localized over GO/HAP-2 nanocomposites and cationic MG.²⁹⁻³⁰Here the π - π stacking interaction between dye and adsorbent also plays major role in the adsorption of MG.

3.1.FTIR Study

Fig. 1c depicts the FTIR spectra of GO, HAP and GO/HAP-2 respectively. Apart from the aromatic C=C skeletal vibration at 1625 cm⁻¹ for sp² domains, as expected, the FTIR spectrum of GO shows the presence of different oxygenated functional groups too such as, C-O stretching mode at 1075 cm⁻¹, C-OH stretching vibration at 1250 cm^{-1 31}, C=O stretching vibration at 1730 cm⁻¹ and O-H stretching vibration at 3415 cm⁻¹. On HAP and GO/HAP-2 the doublet with one peak at 608 cm⁻¹ and another with 567 cm⁻¹ are attributed to the bending vibration of PO₄³⁻³². The sharp peaks at 1039 cm⁻¹ and 1092 cm⁻¹ are considered to be the breathing modes of P-O stretching vibration. The broad peak at 3458 cm⁻¹ was ascribed to the presence of -OH, possibly due to adsorbed water. The emergence of the characteristic peaks of HAP in the spectra of GO/HAP-2 suggesting the successful conjugation of HAP onto the surface of GO. However, Compared to GO, GO/HAP-2 contains no vibration attributed to C-O stretching at 1075 cm⁻¹ and C-OH vibration at 1250 cm⁻¹. In addition, the relative intensity of C=O stretching vibration is decreased from neat GO. Such phenomena observed in the spectrum of GO/HAP-2 promise that GO are partially reduced. The FTIR spectra of MG adsorbed GO/HAP-2 was analyzed to know the adsorption as shown in fig. S2 (supporting information). The appearance of bands at 1576 and 1401 cm⁻¹ confirms the adsorption of MG onto GO/HAP-2 nanocomposites.

3.2. Raman Study

Raman spectra of HAP as shown in Fig. 1d shows narrow band at around 957-961 cm⁻¹, confirming the symmetric, non-degenerated and stretching mode of PO_4^{3-} ions in the stechiometric HAP with Ca/P molar ratio of 1.66 and/or carbonate apatite.³³ The systematic bending, v_2 , mode of PO_4^{3-} is present in the range 400-450 cm⁻¹. Similarly the characteristics peak of GO at 1348 cm⁻¹ and 1591 cm⁻¹ are assignable to sp³ D band and sp² G band respectively³⁴ and the value of I_D/I_G is calculated as 1.02. However after conjugation the intensity and position of bands of GO/HAP-2 are found different from native HAP as well as GO and the value of I_D/I_G is calculated as 0.96. The decrease in the value of I_D/I_G indicates that the GO was slightly reduced. The reduction of GO was also discussed by Zhuo et al³⁴ using Raman study. Moreover, the slight change in the position of Raman bands in GO/HAP-2 shows the interaction between GO and HAP.

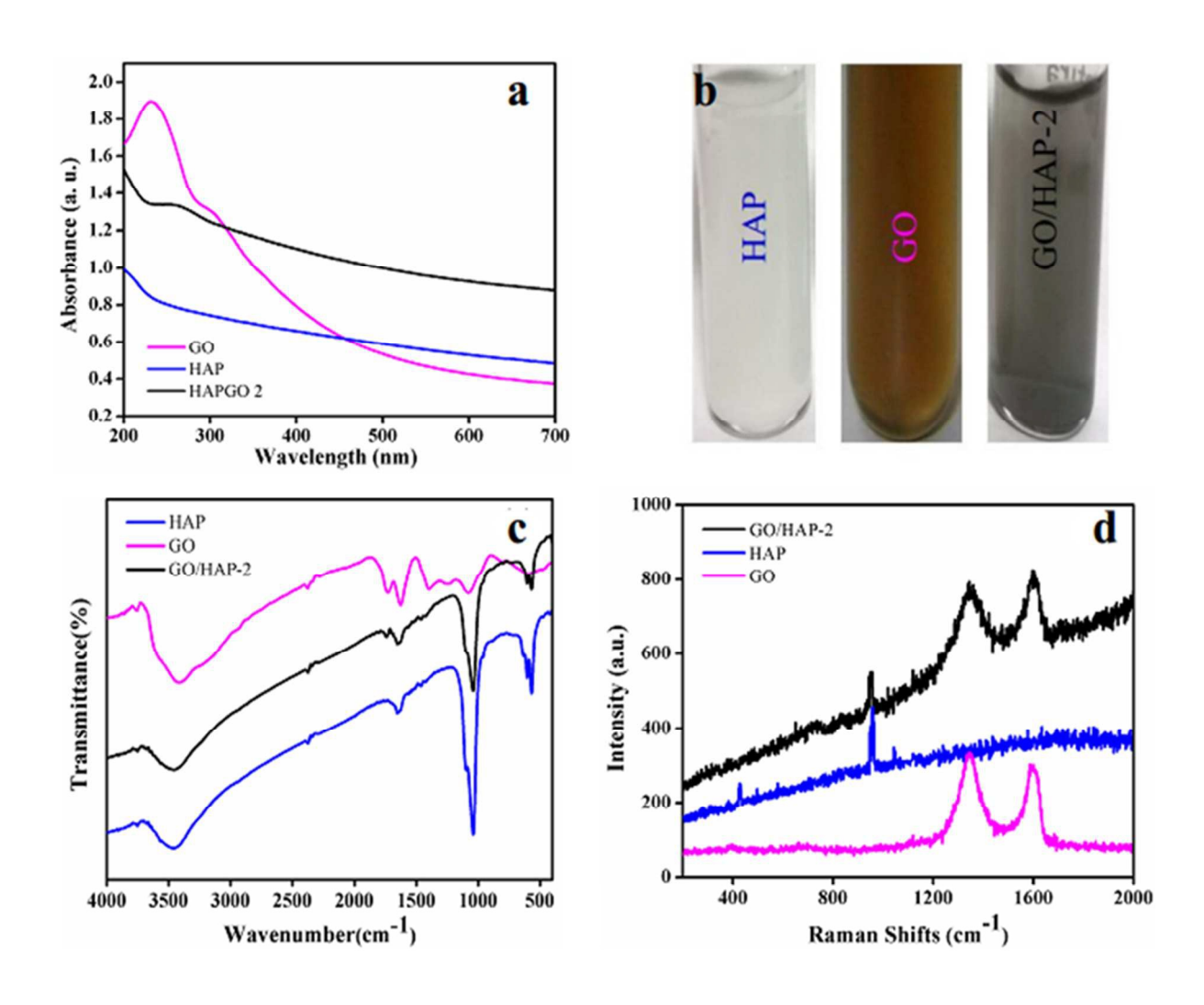


Fig. 1 UV-VIS absorption spectra of GO, HAP and GO/HAP nanocomposite (a) and their corresponding photographs (b). FTIR spectra of HAP, GO and GO/HAP-2 (c), Raman spectra of HAP, GO and GO/HAP-2 (d).

3.3. XRD study

The phase structure and purity of GO, HP and GO/HAP-2 were investigated by wide angle XRD as demonstrated in Fig. 2a. The sharp diffraction peak at around 2θ = 12.0 corresponds to 002 reflection for stacked GO sheets. However diffractogram obtained for HAP presents several

peaks in a wide range of spectrum. The characteristic peaks of HAP reveal the presence of calcium HAP.³⁵ However no diffraction band for GO were seen in the xrd pattern of GO/HAP-2, indicating the destruction of regular layer stacking of GO sheets ³⁶ by the incorporation of HAP nanograins or the peak of GO may be covered by the strong peaks of HAP.

3.3. TGA analysis

The HAP, GO and GO/HAP-2 were subjected to TGA analysis to verify FESEM observations and the obtained curves are depicted in Fig. 2b. Due to high thermal stability HAP shows slow and overall 5.5 % weight loss during the heating under nitrogen atmosphere. The first phase weight loss (4.2%), in the temperature range up to 395 °C corresponds to surface adsorbed water molecules. However the second phase weight loss (1.3%) in the temperature range above 395 °C might be attributed to the loss of intra crystalline water along with the decomposition of PO₄³ions.³⁷ In contrast, it is observed that GO start to lose weight upon early stage of temperature (~ 100 °C) and fast weight loss (37.3%) occurred at 190 °C, which corresponds to the volatilization of adsorbed water in its π -stacked structure. Next the weight loss reached to 45.4% at 350 °C, which is attributed to the decomposition of the epoxy and hydroxyl groups. These results demonstrate that the graphite was successfully converted to thin layered GO structures. For GO/HAP-2, the first weight loss (12.2%) up to 350 °C was observed which could be assigned to the decomposition and vaporization of various oxygen containing functional groups.³⁸ The further weight loss (3.4%) might be due to the loss of intra crystalline water along with the decomposition of PO₄³⁻ ions.

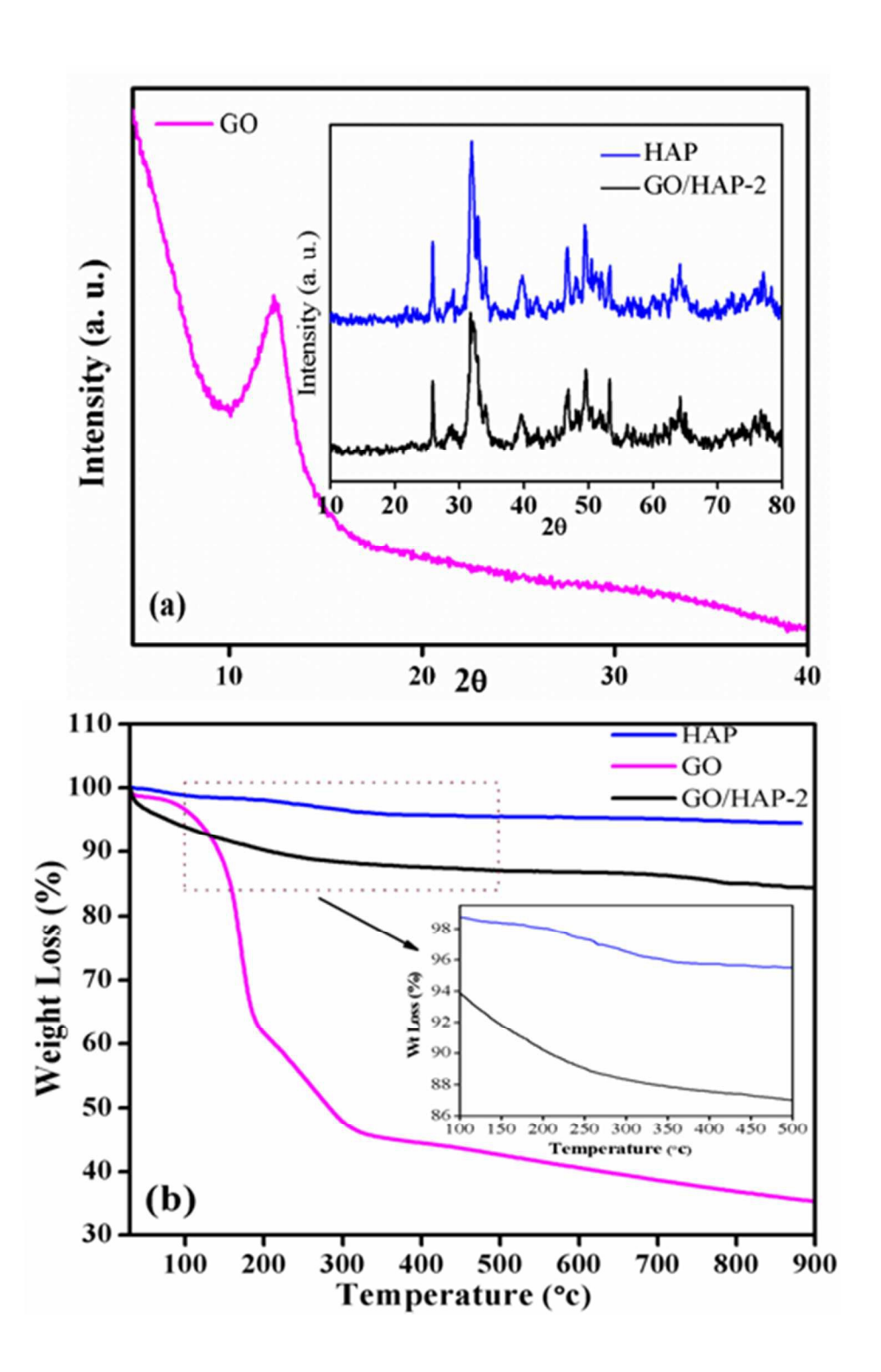


Fig. 2 XRD spectra of HAP, GO and GO/HAP-2 (a), TGA analysis of HAP, GO and GO/HAP-2 (b).

3.4. FESEM study

The morphology of HAP, GO and GO/HAP composites was examined by FESEM and the obtained images are shown in Fig. 3. It could be seen that the shapes of GO looks like flakes of leaves³⁹ as shown in Fig. 3a. This type of morphology is also seen in the AFM image of GO (Fig. S3, supporting information). Fig. 3b depicts the FESEM image of HAP which indicates the rice grain morphology. It is visualized that GO possesses ample amount of cavities formed between GO leaves which permit free entry of HAP into the inner layers. The free entry of HAP results in strong conjugation between HAP and GO as shown in Fig. 3(c-e). The high magnification images of GO/HAP-2 and GO/HAP-3 are shown in Fig. S4 (supporting information). In GO/HAP-1 the graphene leaves are visible with partly coverage with HAP. With increasing HAP content as in GO/HAP-2 nanocomposites, the cavities of GO becomes filled but in GO/HAP-3, GO was completely covered with by HAP. GO/HAP-2 show better adsorption activity compared to GO/HAP-1 and GO/HAP-3 towards the adsorption of MG.

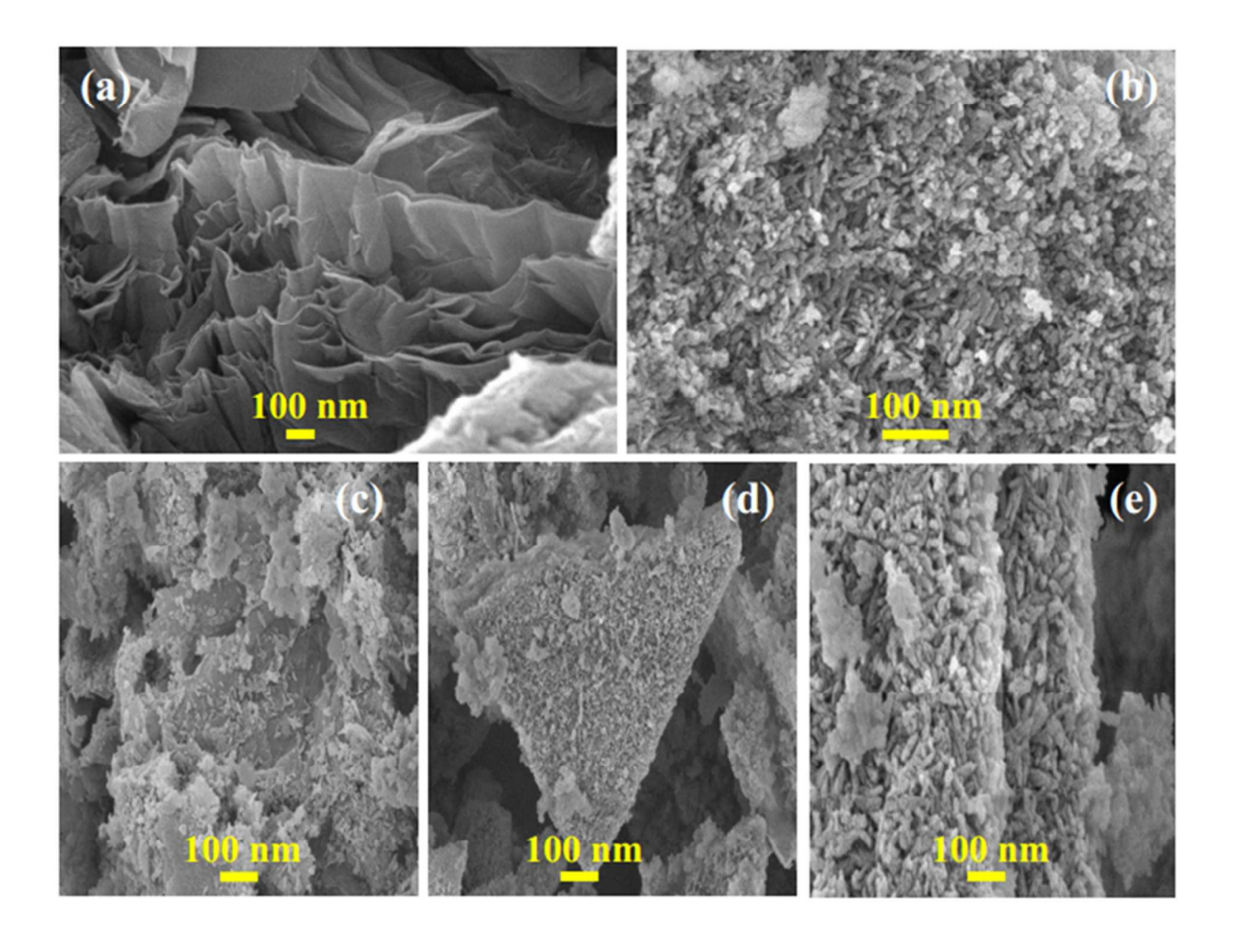


Fig. 3 FESEM image of GO (a), HAP (b), GO/HAP-1 (c), GO/HAP-2 (d), GO/HAP-3 (e).

3.5. Surface area analysis

The textural properties of GO, HAP and GO/HAP-2 nanocomposite were investigated from their N_2 adsorption/desorption isotherms (Fig. S5, supporting information) and the relative parameters are displayed in table T1 (supporting information). Compared to GO (119.13 m²g⁻¹), the BET surface area of GO/HAP-2 (91.189 m²g⁻¹) decreased. This is owing to the smaller specific surface area of HAP (39.028 m²g⁻¹).

3.7. Effect of adsorbent dose on adsorption of MG

The effect of adsorbent dose on MG adsorption by GO/HAP-2 was investigated and the result is shown in fig. 4a. Experimental data reveal that MG adsorption was found to be minimum (90.2%) at an adsorbent dose of 0.004g and increased to 99.49% at an adsorbent dose of 0.01g. As we further increased GO/HAP-2 dose up to 0.016 g, the adsorption becomes almost constant with maximum adsorption of 99.69%. The increase in adsorption of MG with increasing adsorbent dose was attributed to the availability of sufficient surface area, and consequently availability of large number of active sites available for MG adsorption. Furthermore, in higher adsorption dose (>0.01 g) the active sites are much more than threshold saturated adsorption point which leads to aggregation of the active sites. Therefore, the optimum adsorbent dose was chosen as 0.01 g.

3.8. Effect of pH

Different solution pH was used to investigate the effect on the adsorption of MG on GO/HAP-2 nanocomposites and the obtained graph is presented in fig. 4b. It can be seen that adsorption efficiency of MG for GO/HAP-2 nanocomposites experienced a steady increase from 89.73% to 98.93% with the increase of the solution pH. The effects of pH on MG adsorption could be explained on the basis of pH_{ZPC} value (7.0) of GO/HAP-2. In pH< pH_{ZPC}, the surface of nanocomposites is positively charged⁴⁰ and it becomes more positively charged with the decrease in pH. This positive environment, in acidic medium, is less favorable for the adsorption of cationic dye, say MG. On the contrary, in pH>pH_{ZPC}, the surface of nanocomposites is negatively charged and so the adsorption of MG was increased, owing to the strong electrostatic interaction between the negatively charged nanocomposites and MG.

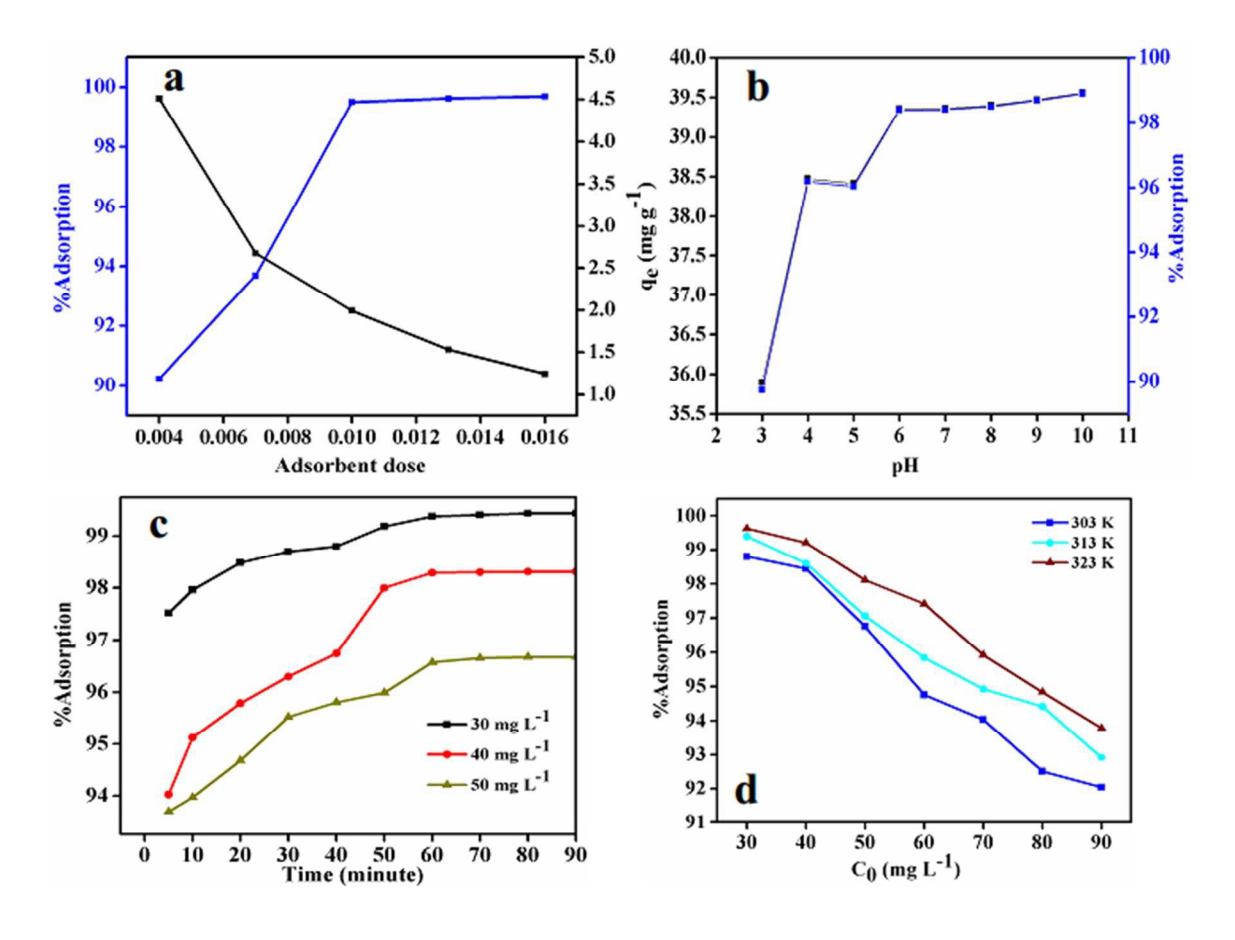


Fig. 4 Effect of mass of adsorbent (a); pH (b); time (c); and initial MG concentration (d). {Temperature: 303 K for (a), (b), and (c), initial MG concentration: 40 mg L⁻¹ (20 mL) for (a) (b) and (d), GO/HAP-2 nanocomposite: 0.01 g for (b), (c), and (d).}

3.9. Effect of contact time: kinetic analysis

The adsorption of MG on GO/HAP-2 nanocomposites was investigated as a function of contact time to determine the suitable time at which the adsorption reaches equilibrium. As we can see, adsorption reached 97.5%, 94.0% and 93.6% within 5 minute for the initial MG concentration of 30, 40 and 50 mg L^{-1} respectively. Thereafter slow adsorption rates were observed till 60 minute and after 60 minute almost static adsorption (%) occurred for all MG concentrations (30, 40 and 50 mg L^{-1}). The static behavior of adsorption after a particular time

have been previously reported^{17,18,42}. SO here the optimum time for adsorption of MG was set to 60 minute in all study. Further the rate that control the adsorption of MG was investigated in terms of pseudo first order, pseudo second order and intraparticle diffusion models⁴³. The first two models are expressed by the equation 4 and 5 respectively.

$$ln(q_e - q_t) = ln q_e - K_1 t$$
 (4)

$$\frac{t}{q_{t}} = \frac{1}{K_{2}q_{e^{2}}} + \frac{t}{q_{e}} \tag{5}$$

Where K_1 (min⁻¹) and K_2 (g mg⁻¹ min⁻¹) are the adsorption rate constants for Pseudo first order and Pseudo second order respectively. q_t and q_e are the adsorption capacity at time t and equilibrium respectively. The related parameters obtained from these models are presented in table 2. As per R^2 values the data exhibits better fit to pseudo second order model than that of pseudo first order model (fig. 5) for all adsorption data. Moreover, the better fit to pseudo second order can be further justified by the point that the calculated q_e for pseudo second order is very close to expected q_e . However these models were not applicable to identify the diffusion mechanism. So the intraparticle mechanism was employed to elucidate the diffusion mechanism⁴⁴. According to this model, the adsorption at any time (q_t) is supposed to be proportional to $t^{1/2}$ rather than the contact time t. The model parameters of intraparticle diffusion were calculated by the equation 6 and listed in table 2.

$$q_t = k_{id} t^{1/2} + c$$
 (6)

Where k_{id} (mg g⁻¹ t^{1/2}) is the intraparticle diffusion rate constant and c (mg g⁻¹) is the intercept of the intraparticle plot. If the value of c is zero, the adsorption till equilibrium is controlled by intraparticle diffusion. The values of C for all adsorption data (30 mg L⁻¹, 40 mg L⁻¹ and 50 mg

 L^{-1}) confirmed the intraparticle diffusion was involved as a part of diffusion but not the sole rate limiting step⁴⁵.

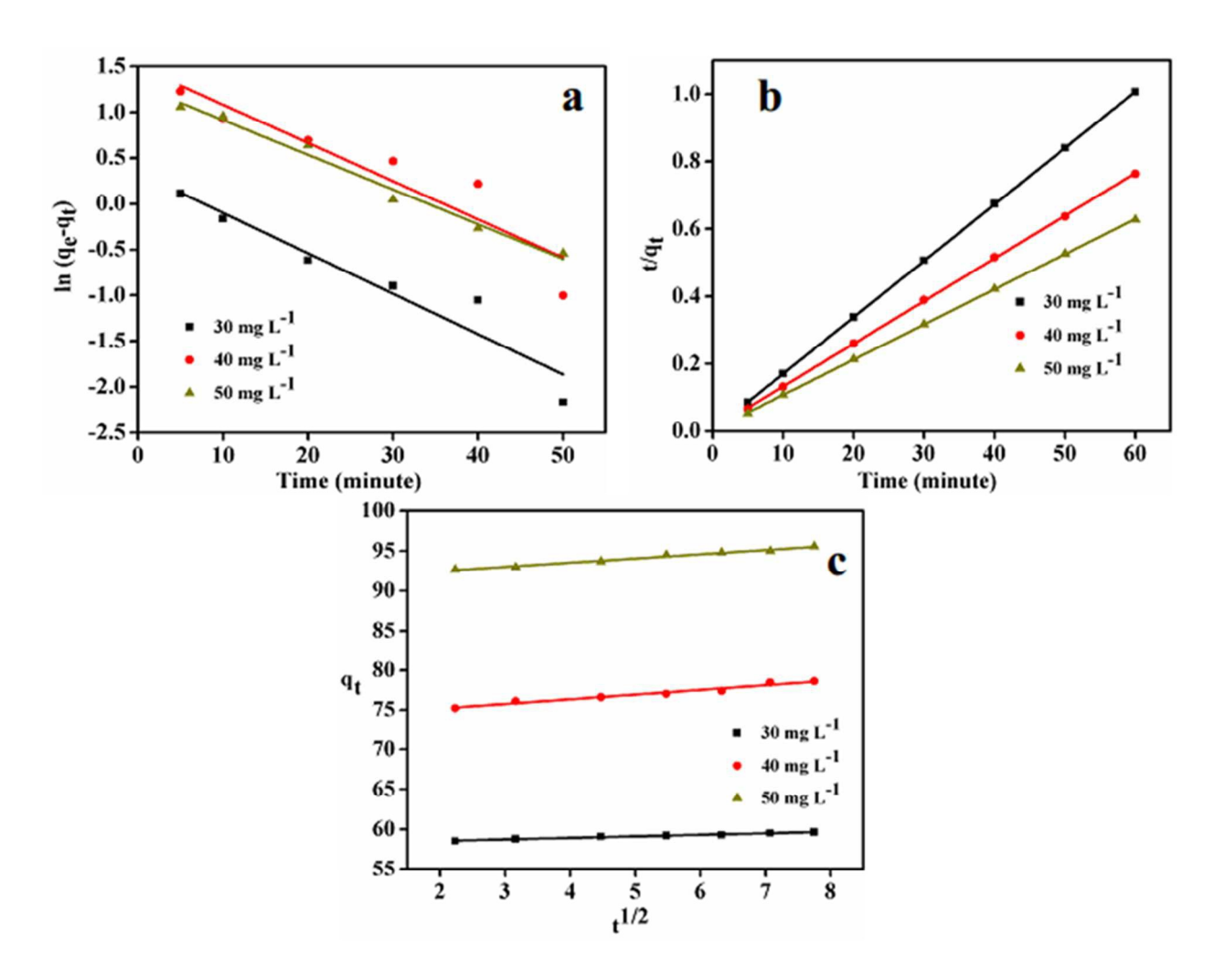


Fig. 5 Pseudo first order (a) Pseudo second order (b) and Intraparticle diffusion (c) kinetic models for MG adsorption. {Temperature: 303 K, GO/HAP-2: 0.01 g}.

Table 2: Adsorption kinetic parameters for MG adsorption on GO/HAP-2^a

MG		Pseudo first order		der	Pseudo second order			Intraparticle diffusion		
	q_e , exp $(mg g^{-1})$	$ {q_e, cal} $ $ (mg g^{-1}) $	R ²	K_1 (min ⁻¹)	q _e , cal (mg g ⁻	R ² 1)	$\frac{K_2}{(g \text{ mg}^{-1} \text{ min}^{-1})}$	${C}$ (mg g ⁻¹)	R ²	$\frac{K_{id}}{(\text{mg g}^{-1} t^{1/2})}$
30 mg L^{-1}	59.62	1.52	0.90	0.0414	59.70	0.999	0.092	58.14	0.97	0.19
$40~\text{mg}~\text{L}^{-1}$	78.63	4.48	0.83	0.0417	78.98	0.999	0.026	73.97	0.96	0.59
$50~\mathrm{mg}~\mathrm{L}^{-1}$	95.57	3.64	0.98	0.0378	95.78	0.999	0.032	91.42	0.98	0.52

cal: calculated; exp: expected.

3.10. Effect of MG dose: isotherm analysis

Adsorption isotherm experiments were performed with MG solution ranging from 30 mg L⁻¹ to 90 mg L⁻¹ with fixed amount of GO/HAP-2 nanocomposites (0.01 g). Results indicated that with increasing the initial MG concentration from 30 mg L⁻¹ to 90 mg L⁻¹, adsorption declined in all tested temperature (fig. 4d). This is because of the saturation of the active sites of the nanocomposites⁴⁶. However the relative increase in the adsorption efficiency with temperature is attributed to the increase in kinetic energy of MG molecules⁴⁷. Freundlich, Hansley and Langmuir isotherm models were exploited to elucidate the adsorption behavior at every tested temperature. The Freundlich and Langmuir isotherms can be best described by the equation 6 and 7 respectively.

$$\ln q_e = \ln K_f + \frac{1}{n} \ln C_e \qquad (6)$$

$$\frac{C_{\rm e}}{q_{\rm e}} = \frac{C_{\rm e}}{q_{\rm 0}} + \frac{1}{K_{\rm l} \ q_{\rm 0}} \tag{7}$$

where K_f (mg g⁻¹) is the Frendluich constant which implies the amount of dye adsorbed, n is the heterogeneity factor, q_0 is the maximum adsorption capacity and K_1 (L mg⁻¹) represents the Langmuir constant related to heat of adsorption^{1,48}. The linear fit for these models and the relative observations are displayed in Fig. 6 and table 3 respectively. As per R² values, the adsorption isotherm is best fitted to Freundlich isotherm. Moreover, the values of K_f were 84.54, 93.40 and 104.44 mg L⁻¹ at 303, 313 and 323 K respectively. The value of K_f increased with increasing temperature, revealing that the adsorption efficiency of MG onto GO/HAP-2 nanocomposites increased with the increase in temperature. On the contrary, the value of 1/n decreased with the increasing temperature but lies in between 0 and 1. The value of 1/n favors the assumption that the type of adsorption is favorable and also reveals a higher likelihood of multilayer adsorption of MG^{48} .

The dimension less separation factor R_L of Langmuir isotherm was used to assess the feasibility of MG adsorption¹. R_L is expressed as

$$R_{L} = \frac{1}{1 + K_{1}C_{0}} \tag{8}$$

The value of R_L indicates the type of isotherm to be favorable (0 < R_L < 1), unfavorable (R_L > 1), linear (R_L = 1) and irreversible (R_L = 0). Results demonstrate that the adsorption of MG at every tested temperature is favorable. In order to get more insight for MG adsorption, Hansley model is

also fitted to the experimental data to find any possibility of multilayer adsorption. The linearised Hansley equation⁴⁸ is expressed by

$$\ln q_e = \left[\left(\frac{1}{n} \right) \ln K \right] + \ln C_e / n$$
 (9)

The correlation coefficient for Hansley isotherm were also fitted well (data not shown here) to the adsorption data implying that multilayer adsorption took place onto GO/HAP-2 nanocomposites. This finding supports the observations of freundlich model.

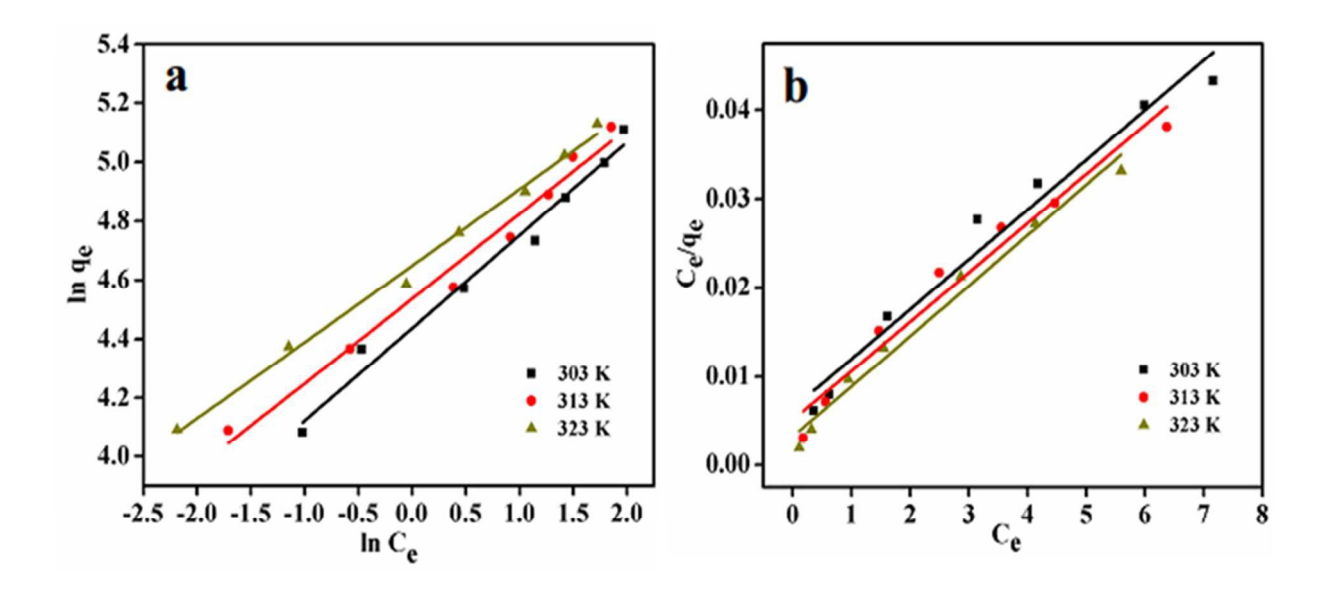


Fig. 6 Freundlich (a) and Langmuir (b) adsorption isotherm for MG adsorption on GO/HAP-2. {Time: 60 minute, Temperature: 303 K, Initial MG concentration: 30–90 mg L⁻¹ (20 mL) and GO/HAP-2: 0.01 g}.

Table 3: Adsorption isotherm parameters for MG adsorption on GO/HAP-2.

	Freundlich			Langmuir			
Temperature	$K_{\rm f}$ (mg g ⁻¹)	R^2	1/n	$q_0 \pmod{g^{-1}}$	R ²	K_l (L mg ⁻¹)	$R_{\rm L}$
303 K	84.54	0.978	0.31	178.5	0.965	0.87	0.03
313 K	93.40	0.977	0.28	180.5	0.960	1.08	0.02
323 K	104.44	0.993	0.25	176.0	0.978	1.77	0.01

3.11Effect of temperature: the thermodynamic study

The effect of different temperatures on the adsorption of MG by GO/HAP-2 nanocomposites was investigated and the obtained graph is presented in Fig. S6 (supporting information). It was observed that as the temperature increased from 303 K to 323 K, adsorption increased. The thermodynamic of adsorption of MG on GO/HAP-2 in terms of change in Gibbs energy (Δ G: kJ mol⁻¹), enthalpy (Δ H: kJ mol⁻¹) and entropy (Δ S: kJ mol⁻¹K⁻¹) were investigated using the known equation⁴⁷.

$$\Delta G = -RT \ln K_c \tag{10}$$

$$\ln Kc = \frac{\Delta S}{R} - \frac{\Delta H}{RT}$$
 (11)

Where R is the gas constant (8.314 J mol K^{-1}), T is temperature (K) and K_c is the distribution coefficient calculated from q_e/C_e . The values of ΔS and ΔH were calculated from the intercepts and slopes of the Van't Hoff plot of ln K_c versus 1/T (Fig. 7a). The results of thermodynamic calculations were listed in table 4. The negative value of ΔG at all temperatures showed that the adsorption process was spontaneous and feasible in nature and the degree of spontaneity increased with increasing temperature. Generally, the value of ΔG gives the information about nature of adsorption⁴⁹. If ΔG is in between -20 and 0 kJ mol⁻¹, the adsorption is physic-sorption while chemi-sorption has a range of -80 to -400 kJ mol⁻¹. Our results as shown in table 4 suggested that the adsorption is physic-sorption. In addition, the positive value of ΔH confirmed the endothermic nature while the positive value of ΔS implied more randomness at the solid solute interface during adsorption. Further, the low value of ΔS revealed that during adsorption there is no remarkable change occurred on entropy⁵⁰.

Table 4: Adsorption thermodynamic parameters for MG adsorption on GO/HAP-2.

MG	Temperature (K)	ΔH (kJ mol ⁻¹)	ΔS (kJ mol ⁻¹ K ⁻¹)	K _c	ΔG (kJ mol ⁻¹)
	303			163.92	-12.84
$30\;mg\;L^{-1}$	313	47.99	0.2	329.85	-15.08
	323			532.28	-16.85
	303			125.91	-12.18
$40\;mg\;L^{-1}$	313	27.67	0.13	140.37	-12.86
	323			249.88	-14.82
	303			59.64	-10.29
$50\;mg\;L^{-1}$	313	22.25	0.1	65.98	-10.90
	323			103.47	-12.45

3.12Recycling Experiments

The adsorption performance of GO/HAP-2 in the recycling experiments was investigated and the time profile of four repeated experiments in the adsorption of MG (20 ml of 40 mg L⁻¹) is shown in Fig. 7b. It can be seen that GO/HAP-2 could be reused without drastic decrease in its adsorption efficiency and 82% adsorption can be obtained in fourth run which proved its feasibility in practical application.

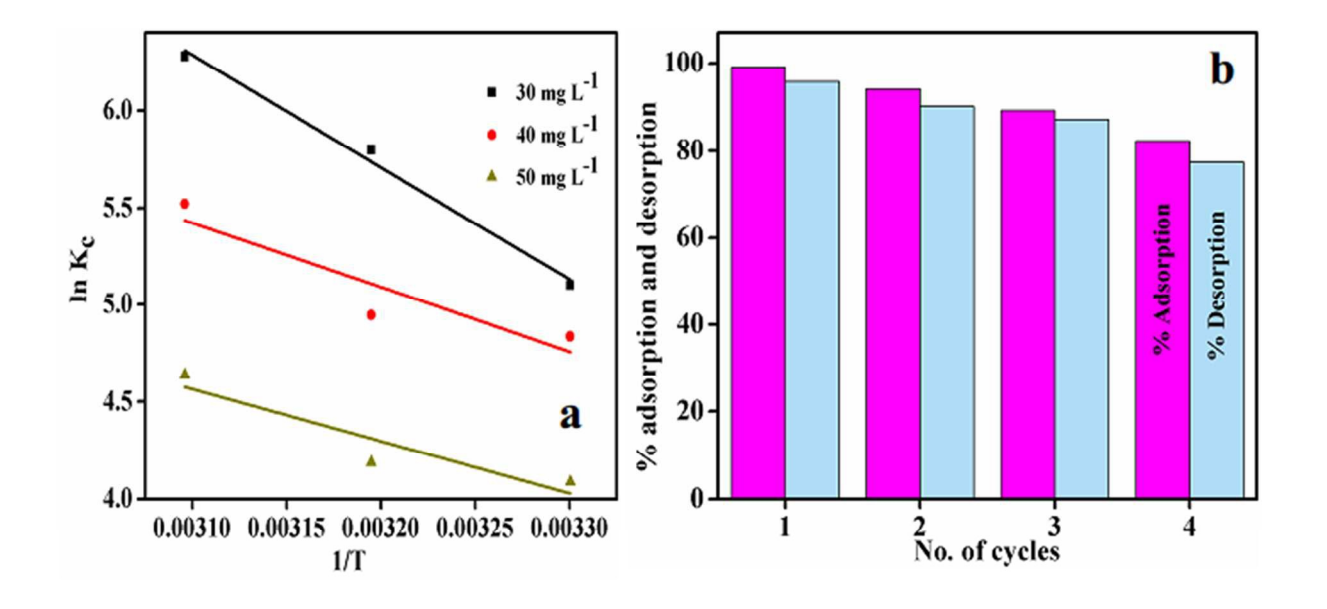


Fig. 7 Van't Hoff plot the adsorption of MG (a) and Adsorption-desorption cycle of MG (b). {Temperature: 303 K for (b), GO/HAP-2: 0.01 g for (a) and (b), Initial MG concentration: 40 mg L⁻¹ for (b)}.

4. CONCLUSION

Hydroxyapatite was conjugated with GO to synthesized GO/HAP-2 nanocomposite which demonstrated an enhanced adsorption efficiency for removal of MG from aqueous phase through electrostatic interaction. The FTIR study proved the adsorption of MG into the GO/HAP-2 nanocomposite. Alkaline condition was favorable for MG adsorption because the PZC of the adsorbent was calculated as 7. The thermodynamic studies revealed that the adsorption was spontaneous and endothermic process.

Acknowledgement

The contents of this research were developed after research bursaries from Indian School of Mines, Dhanbad during the doctoral studies of the first author. Therefore the authors would like to express their gratitude to Indian School of Mines, Dhanbad, Jharkhand.

References

- [1] T. K. Mahto, S. Chandra, C. Haldar and S. K. Sahu, RSC Adv., 2015, 5, 47909–47919.
- [2] T. K. Mahto, A. R. Chowdhuri and S. K. Sahu, J. Appl. Polym. Sci., 2014, 131, 40840–40848.
- [3] F. J. M. Jimeno, F. Garcia, J. I. Paredes, A. M. Alonso and J. M. D. Tascon, Carbon, 2015, 8, 137-147.
- [4] Y. Li, J. Sun, Q. Du, L. Zhang, X. Yang, S. Wu, Y. Xia, Z. Wang, L. Xia and A. Cao, Carbohydr Polym, 2014, 102, 755–761.
- [5] C. H. Huang, K. P Chang, H. D Ou, Y. C Chiang and C. F Wang, Microporous Mesoporous mater., 2011, **141**,102–109.
- [6] R. Hazzaa and M. Hussein, Environm. Tech. Innovation, 2015, 4, 36–51.
- [7] F. Wang, F. Wang, D. Zhu and W. Chen, Environ. Pollut., 2015, **196**, 371–378.
- [8] D. Gu and J. B. Fein, Colloids and Surfaces A: Physicochem. Eng. Aspects, 2015, **481**, 319–327.
- [9] H. Li and X. Cui, Int. J. Hydrogen Energy, 2014, **39**, 19877–19886.

- [10] F. Chen, P. Huang, Y. J. Zhu, J. Wu, C. L. Zhang and D. X. Cui, Biomaterials, 2011, 32, 9031–9039.
- [11] S. S. Samandari, S. S. Samandari, N. Nezafati and K. Yahya, Journal of Environmental Management, 2014, 146, 481–490.
- [12] C. S. Sundaram, N. Viswanathan and S. Meenakshi, Bioresource Technology, 2008, **99**, 8226–8230.
- [13] F. Ye, H. Guo, H. Zhang and X.He, Acta Biomaterialia, 2010, 6, 2212–2218.
- [14] Y. J. Guo, Y. Y. Wang, T. Chen, Y. T. Wei, L. F. Chu and Y. P. Guo, Mater. Sci. Eng., C, 2013, **33**, 3166–3172.
- [15] F. Ye, H. Guo, H. Zhang and X. He, Acta Biomaterialia, 2010, 6, 2212–2218.
- [16] W. Wei, R. Sun, J. Cui and Z. Wei, Desalination, 2010, 263, 89–96.
- [17] R. M. Mohamed, and E. S. Baeissa, Appl. Catal., A, 2013, 464, 218–224.
- [18] K. Lin, J. Pan, Y. Chen, R. Cheng and X. Xu, J. Hazard. Mater., 2009, 161, 231–240.
- [19] H. Hou, R. Zhou, P. Wu, and L. Wu, Chem. Inj. J, 2012, **211**, 336–342.
- [20] X. Y. Zhao, Y. J. Zhu, J. Zhao, B. Q. Lu, F. Chen, C. Qi, and J. Wu, J Colloid Interface Sci., 2014, 416, 11–18.
- [21] M. Li, Q. Liu, Z. Jia, X. Xu, Y. Cheng, Y. Zheng, T. Xi, and S. Wei, Carbon, 2014, 67, 185–197.

- [22] F. Gao, C. Xu, H. Hu, Q. Wang, Y. Gao, H. Chen, Q. Guo, D. Chen, and D. Eder, Mater Lett, 2015, **138**, 25–28.
- [23] S. Nethaji, A. Sivasamy, G. Thennarasu, and S. Saravanan, J. Hazard. Mater., 2010,181, 271–280.
- [24] Y. Song, Z. He, H. Hou, X. Wang and L. Wang, Electrochim. Acta, 2012, 71, 58–65.
- [25] G. He, W. Liu, X. Sun, Q. Chen X. Wang, and H. Chen, Mater. Res. Bull., 2013, **48,** 1885–1890.
- [26] Y. Liu, H. Zhong, L. Li and C. Zhang, Mater. Res. Bull., 2010, 45, 2036–2039.
- [27] V. Dhand, K.Y. Rhee, and S. J. Park, Mater. Sci. Eng., C, 2014, **36**, 152–159.
- [28] S. Baradaran, E. Moghaddam, W. J. Basirun, M. Mehrali, M. Sookhakian, M. Hamdi, M. R. N. Moghaddam, and Y. Alias, Carbon, 2014, 69, 32–45.
- [29] N. Barka, S. Qourzal, A. Assabbane, A. Nounah, and Y. A. Ichou, J. Saudi Chemical Society, 2011, 15, 263-267.
- [30] H. Hou, R. Zhou, P. Wu and L. Wu, Chem. Eng. J., 2012, 211, 336–342.
- [31] D. C. Marcano, D. V. Kosynkin, J. M. Berlin, A. Sinitskii, Z. Sun, A. Slesarev, L. B. Alemany, W. Lu, and J. M. Tour, 2010, 4, 4806–4814.
- [32] F. Gao, C. Xu, H. Hu, Q. Wang, Y. Gao, H. Chen, Q. Guo, D. Chen and D. Eder, Mater. Lett., 2015, 138, 25–28.
- [33] A. M. Sofronia, R. Baies, E. M. Anghel, C. A. Marinescua, and S. Tanasescua, Mater. Sci. Eng., C, 2014, 43, 153–163.
- [34] Q. Zhuo, Y. Zhang, Q. Du, C. Yan, J Colloid Interface Sci., 2015, 457, 243-247.

- [35] Y. Fu, H. Chen, X. Sun and X. Wang, Appl. Catal., B: Environmental, 2012, 111, 280–287.
- [36] C. Cui, Y. Wanga, D. Liang, W. Cuib, H. Hu, B. Lua, S. Xua, X. Lia, C. Wang and Y. Yang, Appl. Catal. B: Environmental, 2014, 158, 150–160.
- [37] M. Hermassi, C. Valderrama, J. Dosta, J. L. Cortina, and N. H. Batis, Chem. Eng. J, 2015, 267, 142–152.
- [38] Y. Song, Z. He, H. Hou, X. Wang and L. Wang, Electrochim. Acta, 2012, 71, 58–65.
- [39] J. Li, D. kuang, Y. Fenga, F. Zhang, Z. Xu and M. Liu, J. Hazard. Mater., 2012, **201**, 250–259.
- [40] P. Raizada, P. Singh, A. Kumar, G. Sharma, B. Pare, S. B. Jonnalagadda, and P. Thakur, Appl Catal A, 2014, **486**, 159–169.
- [41] J. Fang, X. Huang, X. Ouyang, and X. Wang, Chem. Inj. J, 2015, 270, 309–319.
- [42] M. T. N. Le, and B. K. Lee, Chem. Inj. J, 2015, 281, 20-33.
- [43] O. Moradi, V. K. Gupta, S. Agarwal, I. Tyagi, M. Asif, A. S. H. Makhlouf, H. Sadegh, and R. S. ghoshekandi, J Ind Eng Chem, 2015, **28**, 294–301.
- [44] A. I. Umar, G. Abdulraheem, S. Bala, S. Muhammad, and M. Abdullahi, Int. Biodeterior. Biodegrad., 2015, **102**, 265–273.
- [45] L. Yu, and Y. M. Luo, J Env. Chem. Eng., 2014, 2, 220–229.
- [46] X. Rong, F. Qiu, J. Qin, H. Zhao, J. Yan, and D. Yang, J Ind Eng Chem, 2015, 26, 354–363.
- [47] M. E. Argun, D. Guclu, and M. Karatas, J Ind Eng Chem, 2014, 20, 1079–1084.

[48] M. S. U. Rehman, M. Munir, M, Ashfaq, N. Rashid, M. F. Nazar, M. Danish, and J. I. Han, Chem. Inj. J, 2013, **228**, 54–62.

[49] X. Jin, B. Yu, Z. Chen, J. M. Arocena, and R. W. Thring, J Colloid Interface Sci.,2014, 435, 15–20.

[50] R. Han, J. Zhang, P. Han, Y. Wang, Z. Zhao, and M. Tang, Chem. Inj. J, 2009, **145**, 496–504.